Multistage interaction of a shock wave and a strong vortex

Shuhai Zhang[a)]
China Aerodynamics Research and Development Center, Mianyang, Sichuan 621000, China

Yong-Tao Zhang[b)]
Department of Mathematics, University of California at Irvine, Irvine, California 92697

Chi-Wang Shu[c)]
Division of Applied Mathematics, Brown University, Providence, Rhode Island 02912

(Received 22 June 2005; accepted 16 August 2005; published online 8 November 2005)

The interaction between a shock wave and a strong vortex is simulated systematically through solving the two-dimensional, unsteady compressible Navier–Stokes equations using a fifth-order weighted essentially nonoscillatory finite difference scheme. Our main purpose in this study is to characterize the flow structure and the generation of sound waves of the shock–strong vortex interaction. The simulations show that the interaction of a shock wave and a strong vortex has a multistage feature. It contains the interaction of the shock wave and the initial vortex, of the reflected shock wave and the deformed vortex and of the shocklets and the deformed vortex. The shocklets are generated by the secondary interaction. Due to the complex reflected shock structure, there exist interactions between the reflected shock waves and the sound waves. Many pressure waves are embedded in the second and third sound waves. © *2005 American Institute of Physics*. [DOI: 10.1063/1.2084233]

I. INTRODUCTION

The interaction between shock waves and vortices is an important phenomenon in aerodynamics and aeroacoustics. When a plane shock wave meets a vortex, disturbance is generated, which propagates along the shock wave and results in its deformation. Behind the curved shock wave, the flow field is compressed and rarefied locally and forms acoustic waves. These interesting phenomena are closely related to the shock–turbulence interaction, which is one of the major sources of noise, and has attracted a lot of attention in the literature.

An early experimental study of shock vortex interaction was carried out by Hollingsworth and Richards.[1] A plane shock wave was generated by a shock tube. As it passed an aerofoil with an attack angle to the flow, a spiral vortex was shed. After the shock wave was reflected by the wall at the end of the shock tube, it traveled back toward the vortex and the interaction between the shock and the vortex took place. Acoustic waves and bending of the shock were observed. It was found that the acoustic wave consisted of four alternating compression and rarefaction regions centered at the transmitted vortex. With a similar apparatus and a Mach–Zehnder interferometer, Dosanjh and Weeks[2] measured the circumferential pressure distribution of the acoustic wave, which later became the benchmark experimental data for a numerical comparison. The experimental results also found that the original vortex was compressed into an elliptical shape. The major axis was approximately equal to the diameter of the initial circular vortex and the ratio of the major to minor axes was approximately equal to the density ratio across the shock wave. Naumann and Hermann[3] used a double-sided shock tube to produce the interaction of a shock wave and a vortex. The flow field for the time evolution of the shock vortex interaction was visualized by a Mach–Zehnder interferometer coupled with a high-speed camera. The experiment revealed that the deformation of the shock wave was either a regular or a Mach reflection, depending on the strength of the shock wave and vortices.

The linear theory to explain the production of sound in a shock vortex interaction was developed by Ribner[4,5] and by Weeks and Dosanjh.[6] Ribner decomposed the vortex into plane sinusoidal shear waves by a Fourier transform and then recombined the plane sound waves produced by the interaction of each shear wave with the shock wave. This analysis resulted in a cylindrical acoustic wave. The circumferential sound pressure presented a quadrupolar character with perfect antisymmetry with respect to the normal of the shock. The result of Ribner[5] agreed well with the antisymmetry component of the interferometric measurement.[2] Weeks and Dosanjh[6] extended the theory of Lighthill[7] and Curle[8] and represented the circumferential pressure as a combination of quadrupole, dipole, and monopole acoustic sources. The monopole part allowed a distortion from the purely antisymmetric pattern. Their prediction for the acoustic waves agreed well with their experimental data. Ting[9] solved the acoustic waves from the linearized equations of the compressible flow and obtained a quadrupolar pressure distribution similar to the result of Ribner.

Guichard *et al.*[10] simulated the flow field in a mixing zone produced by shock interaction with a single vortex or a pair of vortices by solving the Navier–Stokes equations us-

a)Electronic mail: zhang_shuhai@tom.com
b)Electronic mail: zyt@math.uci.edu
c)Author to whom correspondence should be addressed. Telephone: 1-401-863-2549. Fax: 1-401-863-1355. Electronic mail: shu@dam.brown.edu

ing a sixth-order compact scheme.[11] The deformation of the shock wave and the formation of the triple point were resolved. The numerical result showed that the vorticity was increased and the vortex was bent according to the curvature of the shock. Ellzey *et al.*[12] and Ellzey and Henneke[13,14] studied extensively the problem of shock–vortex interaction. The unsteady compressible Euler equations were solved using a fourth-order flux-corrected transport algorithm of Boris and Book.[15,16] In Ref. 12 the authors examined the effect of different strengths of vortices and shock waves. Their simulation confirmed the quadrupolar nature of the acoustic waves that were generated in the interaction and showed that a strong vortex could distort the incident shock wave and form regular or Mach reflections, depending on the strength of the shock. The reflected shock wave merged with the acoustic wave and resulted in an acoustic wave consisting of a strong compression region near the shock front. In Ref. 13 the authors introduced their earlier results[17] that the shock compressed the originally circular vortex into an elliptical vortex. They studied the effect of the compressed vortex on the formation of sound waves. The result showed that an isolated elliptical vortex could produce similar sound waves as that of shock–vortex interaction. Inoue and Hattori[18] studied the sound generation through simulating the shock interaction with a single vortex or a pair of vortices by solving the two-dimensional Navier–Stokes equations using a sixth-order compact scheme of Lele.[11] They obtained the first and second acoustic waves, both of which have a quadrupolar nature. In the interaction of a shock wave with a pair of vortices, the third and fourth acoustic waves were observed. Although neither the third nor the fourth acoustic wave was observed in the interaction of a shock with a single vortex, the authors suspected that this was due to the limitation of the computational domain and the short simulation time. Later, Inoue[19] performed a numerical simulation with a larger domain and for a longer time, and observed the third sound wave.

Using a fourth-order weighted essentially nonoscillatory (WENO) scheme[20] to solve the two-dimensional Euler equations, Grasso and Pirozzoli[21] simulated the shock vortex interaction problem with an extensive range of strengths for both the shock wave and the vortex. They classified the interaction into three types, depending on the deformation of the shock. The first type is a weak interaction in which the shock is not significantly distorted. The second type is a strong interaction with a regular reflection. The last type is a strong interaction with a Mach reflection. Corresponding regions were divided in terms of the strengths of shock waves and vortices. The acoustic generation evolved in three stages, depending on the shock interacting with the forepart of the vortex, interacting with the rear part of the vortex, and leaving the vortex. The sound wave appeared in bipolar patterns in the first stage and changed to a quadrupolar behavior in the second stage. Erlebacher *et al.*[22] simulated shock interaction with a transverse vortex, emphasizing on a detailed study of disturbance propagating along the shock and indicating that the nonlinear effect became more important for a stronger vortex interacting with a fixed shock.

All of the above studies were focused on the sound generation at relatively weak vortices. As the vortex becomes stronger, it produces a stronger disturbance to the shock wave, which results in stronger reflected shock waves. These reflected shock waves may interact with the deformed vortex to form a secondary interaction. Both Pirozzoli *et al.*[23] and Inoue *et al.*[24,25] studied the interactions of shock waves and vortex pairs with strong intensity. In Ref. 23, Pirozzoli *et al.* studied the flow pattern and classified the shock structure into five types. Their results indicated that the generation of sound waves was influenced by the interaction of shock waves with the vortex pair as well as the vorticity dynamics related to the coupling of the pair. In Ref. 25 Inoue *et al.* focused on the study for the separation of the reflected shock waves by the second vortex and found that there were more sound waves and a complex flow field. Barbosa and Skews[26] studied the shock vortex interaction experimentally in a bifurcated shock tube as well as numerically by solving the two-dimensional Euler equations. The vortex was shed by one of the shocks passing through a wedge and then interacting with another shock generated by the bifurcated shock tube. They observed the "tertiary shocklets" between the vortex core and the wall of the wedge. The pressure spiked at the position of the focused cusp where the slope of the shock front is discontinuous. The comparison between the experimental and numerical results was very good. Rault *et al.*[27] also studied shock vortex interactions with a strong vortex numerically, by solving the Euler equations using Marquina's scheme[28] and found that the interaction of strong shock waves with vortices resulted in the breakdown of the vortices.

Our purpose in this paper is to study the details of the flow structure and sound generation for the interaction of a shock wave with a strong vortex, through simulating the two-dimensional Navier–Stokes equations using the fifth-order WENO scheme of Jiang and Shu.[29] We find that the interaction of a shock wave with a strong vortex has a multistage feature. The strong reflected shock wave interacts with the deformed vortex, which results in the formation of shocklets near the vortex center. The reflected shock wave and the shocklets interact with the deformed vortex. Each stage of the interaction results in an increase of the vorticity and deformation of the vortex. The paper is organized as follows: in Sec. II, the physical model, numerical scheme, and grid generation are introduced. In Sec. III, a numerical example is provided to validate our code and to test its grid sensitivity. In the fourth section we present numerical results and a discussion for the interaction of a shock wave with a strong vortex. The details of the multistage feature of a shock–strong vortex interaction are discussed. The last section contains concluding remarks.

II. MATHEMATICAL FORMULATION AND NUMERICAL PROCEDURE

A. The physical model

Following the simulation of Inoue and Hattori,[18] the interaction of a shock wave with an isolated vortex is simu-

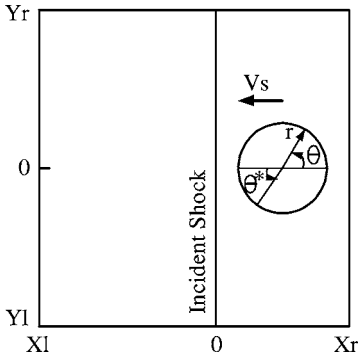

FIG. 1. Schematic diagram of the flow model.

lated in this paper. Figure 1 is a schematic diagram of the flow model. The computational domain is prescribed to be rectangular

$$x_l \leqslant x \leqslant x_r, \quad y_l \leqslant y \leqslant y_r.$$

In our simulation, $x_l=-30$, $x_r=10$, $y_r=-y_l=20$. For the convenience of increasing the resolution of the incident shock wave by a locally refined grid, the shock wave is set to be stationary at $x=0$. The vortex moves from right to left at a speed of V_s.

The initial value of the vortex parameters[18] is set as follows: tangential velocity, $u_\theta(r)=M_v r e^{(1-r^2)/2}$; radial velocity, $u_r=0$; pressure, $p(r)=1/\gamma(1-(\gamma-1)/2M_v^2 e^{1-r^2})^{\gamma/(\gamma-1)}$; density, $\rho(r)=(1-(\gamma-1)/2M_v^2 e^{1-r^2})^{1/(\gamma-1)}$, where $r=\sqrt{(x-x_v)^2+(y-y_v)^2}$, with the initial vortex center $(x_v,y_v)=(4.0,0.0)$. M_v is the strength of the vortex, and $\gamma=1.4$ is the ratio of specific heats. Other quantities can be obtained from the quantities prescribed above. For example, the initial vorticity can be obtained as $\omega(r)=M_v(2-r^2)e^{(1-r^2)/2}$. It is noted that the total circulation of this vortex is zero and the effect of the vortex is negligibly small beyond $r=4$ [see also Figs. 2(a) and 2(b) of Ref. 18].

B. The numerical method

The fifth-order finite difference WENO scheme developed by Jiang and Shu[29] is used to simulate the following two-dimensional unsteady compressible Navier–Stokes equations:

$$U_t + F(U)_x + G(U)_y = \frac{1}{\mathrm{Re}}[F_v(U)_x + G_v(U)_y], \tag{1}$$

where $U=(\rho,\rho u,\rho v,e)^T$, $F(U)=[\rho u,\rho u^2+p,\rho uv,u(e+p)]^T$, $G(U)=[\rho v,\rho uv,\rho v^2+p,v(e+p)]^T$, $F_v(U)=(0,\tau_{xx},\tau_{xy},u\tau_{xx}+v\tau_{xy}+q_x)^T$, $G_v(U)=(0,\tau_{xy},\tau_{yy},u\tau_{xy}+v\tau_{yy}+q_y)^T$. Here ρ is the density, (u,v) is the velocity, e is the total energy, p is the pressure, which is related to the total energy by $e=p/(\gamma-1)+\frac{1}{2}\rho(u^2+v^2)$, the ratio of specific heats $\gamma=1.4$. Re is the Reynolds number defined by $\mathrm{Re}=\rho_\infty a_\infty R/\mu_\infty$, where ρ_∞, a_∞, and μ_∞ are the density, sound speed, and viscosity for the mean flow in front of the shock wave and R is the radius of the vortex core defined by the distance from the vortex center to the location where the tangential velocity attains its maximum. τ_{ij} and q_j (where $i,j=1$ for x and $i,j=2$ for y) are the stress tensor and the heat flux, respectively, and are given as

$$\tau_{ij}=\mu\left(\frac{\partial u_i}{\partial x_j}+\frac{\partial u_j}{\partial x_i}-\frac{2}{3}\delta_{ij}\frac{\partial u_k}{\partial x_k}\right), \quad q_j=\frac{\mu}{(\gamma-1)\mathrm{Pr}}\frac{\partial T}{\partial x_j},$$

where $\mathrm{Pr}=0.75$ is the Prantl number, $\mu=T^{3/2}(1+c)/(T+c)$ is the viscosity computed by the Sutherland law, with $c=110.4/T_\infty$ and $T_\infty=300$, and $T=\gamma p/\rho$ is the temperature. In our calculation, a smooth, nonuniform tensor-product grid

$$\xi=\xi(x), \ \eta=\eta(y)$$

is used, where the physical grid (x_i,y_j) is not uniform, but the computational grid (ξ_i,η_j) is uniform, and the grid transform functions $\xi(x)$ and $\eta(y)$ are monotone, invertible, and smooth (having at least five continuous derivatives for our fifth-order method).

The nonlinear first derivative terms of the Navier–Stokes equations are discretized by the fifth-order finite difference WENO scheme. It has fifth-order accuracy in smooth regions. The solution is essentially nonoscillatory and gives sharp shock transitions near discontinuities. We refer to Refs. 29 and 30 for more details.

The viscous terms are discretized by fourth-order central differences and the time derivative is discretized by the third-order TVD Runge–Kutta method of Shu and Osher.[31] We again refer to Ref. 30 for more details.

C. The grid generation

We have used a series of grids to make sure that we have enough numerical resolution for the flow features for which we are looking. The final computational results are obtained on a nonuniform tensor product mesh of 1280×960 grid points. The grid transformation is given analytically as

$$x(\xi)=x_l[\xi-\alpha_1\xi(1-\xi)e^{-\alpha_2\xi}], \quad \xi\in[0,1],$$

$$y(\eta)=y_r[\eta-\beta_1\eta(1-\eta)e^{-\beta_2\eta}], \quad \eta\in[0,1],$$

where $\alpha_1=0.905$, $\beta_1=0.92$, and $\alpha_2=\beta_2=1.0$. This grid is refined near $x=0$ and $y=0$ and is approximately uniform far away from them. The finest mesh sizes are $\Delta x\approx0.00365$ and $\Delta y\approx0.0035$ near the coordinate axes, and the coarsest meshes are located near the boundaries, with mesh sizes $\Delta x\approx0.05$ and $\Delta y\approx0.056$. This guarantees good resolution of the shock, vortex structure, and sound waves for the problems considered in this paper.

In our simulation, the Mach number of the shock wave is prescribed to be either $M_s=1.05$ or $M_s=1.2$. The interaction corresponds to a regular reflection for $M_s=1.05$ and a Mach reflection for $M_s=1.2$. The Mach number of the vortex is set from 0.5 to 1.00. The Reynolds number is $\mathrm{Re}=800$. In Table I we list the parameters used in our simulation.

III. VALIDATION OF THE CODE AND SENSITIVITY TO THE GRID

The code of the fifth-order finite difference WENO scheme was written originally by Jiang and Shu[29] and has been modified numerous times for different applications. The method and the code have been validated in many papers,

TABLE I. Parameters of shock waves and strong vortices for the simulation.

Case	M_s	M_v	Re	Case	M_s	M_v	Re
A	1.2	1.00	800	F	1.05	1.00	800
B	1.2	0.80	800	G	1.05	0.80	800
C	1.2	0.70	800	H	1.05	0.70	800
D	1.2	0.60	800	I	1.05	0.60	800
E	1.2	0.50	800	J	1.05	0.50	800

including the simulation of strong shocks and the Rayleigh–Taylor instability problem for Euler and Navier–Stokes equations;[29,32,33] see also Ref. 34 for the simulation of the interaction between shock waves and longitudinal vortices using ENO schemes.

For the shock vortex interaction problem considered in this paper, since we are interested in the details of the sound generation, and the sound wave generated by the interaction is very weak comparing with the pressure jump across the shock, a good resolution of the detailed flow structures requires a high-order, nonoscillatory scheme with enough grid resolution.

In order to gauge the resolution of our code, we repeat the case "c" in Inoue and Hattori.[18] The Mach number of the shock is $M_s=1.2$. The strength of the vortex is $M_v=0.25$. We run the code twice corresponding to the two grids of 640×480 and 1280×960 points. The circumferential sound pressures obtained from these two grids are identical visually (hence we only plot the result of the fine mesh with 1280×960 points), and they agree well with the result in Ref. 18; see Fig. 2.

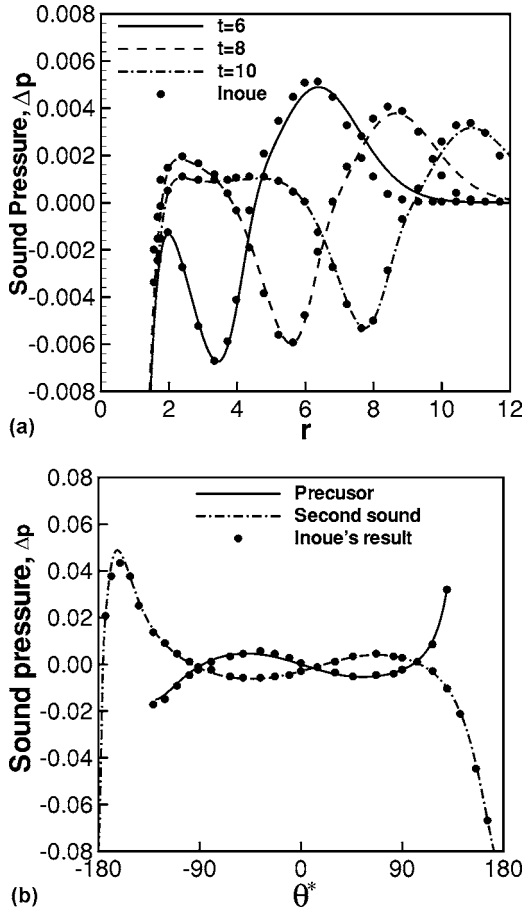

FIG. 2. Comparison of the sound pressure. $M_s=1.2$, $M_v=0.25$. Lines: our simulation with 1280×960 points; symbols: the results in Inoue and Hattori (Ref. 18). (a) Radial distribution; (b) circumferential distribution.

IV. NUMERICAL RESULTS

In this section, the detailed shock structure generated by the interaction is discussed. It is shown that the interaction of a shock wave and a strong vortex has a multistage feature. In Sec. IV B, we discuss the deformation of the vortex in a multistage interaction. The related mechanism of sound generation is discussed in Sec. IV C.

A. The shock structure

The deformation of the incident shock wave in the interaction of a shock wave and a single vortex is very important and has been extensively studied in the literature.[12–14,18,19,21] Most of the previous studies focused on the interaction of a shock wave and weak vortices. The reflected shock wave is weak and cannot interact with the deformed vortex. However, as the strength of the vortex increases, the vortex generates a stronger disturbance to the shock wave. The reflected shock waves become stronger and may interact with the deformed vortex, resulting in a secondary interaction.

1. The shock structure of case A

The evolution of the flow structure for case A is shown in Fig. 3. The pictures are shadowgraphs (contours of $\nabla^2\rho$) that are sensitive to the density gradient. They emphasize the discontinuities including the slip lines and are good at providing the main features of the flow field, especially the shock waves and the slip lines. The shock wave structure is schematically presented in Fig. 4. The reflected shock wave is a Mach reflection for $t\geqslant8.0$. It agrees with the previous result in Ref. 18 for a weak vortex. However, the details of the shock structure in the downstream of the incident shock wave, especially in the near region of the vortex center, are totally different with that for a weak vortex. The interaction of a shock wave and a strong vortex in case A takes places in more stages that were not observed in previous studies.

The first-stage interaction takes place between the incident shock wave and the initial vortex. As the incident shock wave passes through the vortex region, it is distorted into an S shape that can be seen in Fig. 3(a). This pattern is similar to those in previous studies.[18,26] However, the vortex of case A is much stronger than that in the previous studies. It produces a stronger disturbance to the incident shock wave[22] and results in the incident shock wave distorted more seriously. Later, a Mach stem, $M1$, two triple points, $T1$ and $T2$, and two reflected shock waves, $R1$ and $R2$, are formed. This pattern is shown in Figs. 3(b) and 4(a). Because the vortex rotates counterclockwise, the deformed incident shock wave $S2$ moves upward. Hence, $T2$ moves upward and meets with $T1$. The reflected shock wave $R2$ passes through the de-

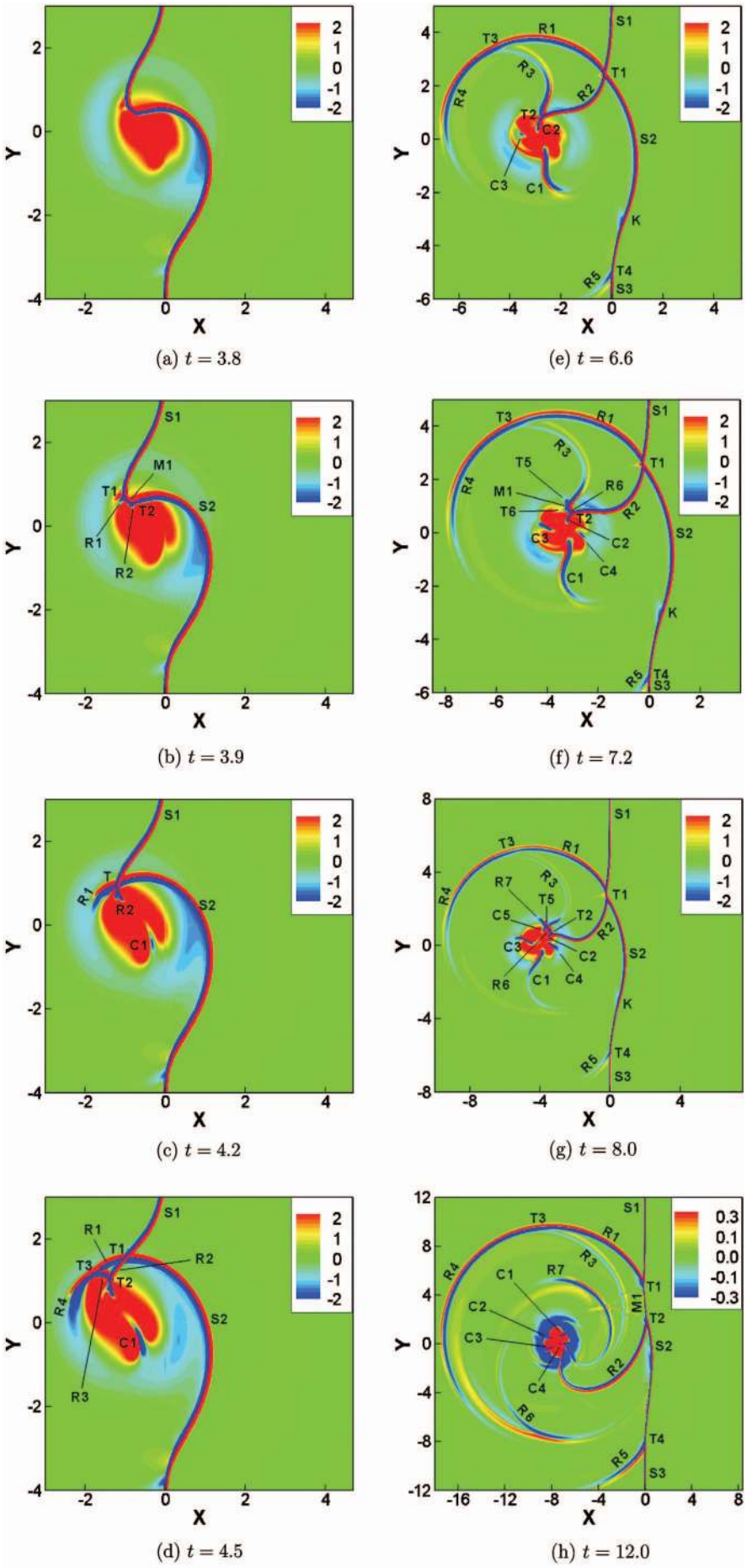

FIG. 3. (Color). The evolution of the flow structure: numerical shadowgraph obtained from $\nabla^2\rho$.

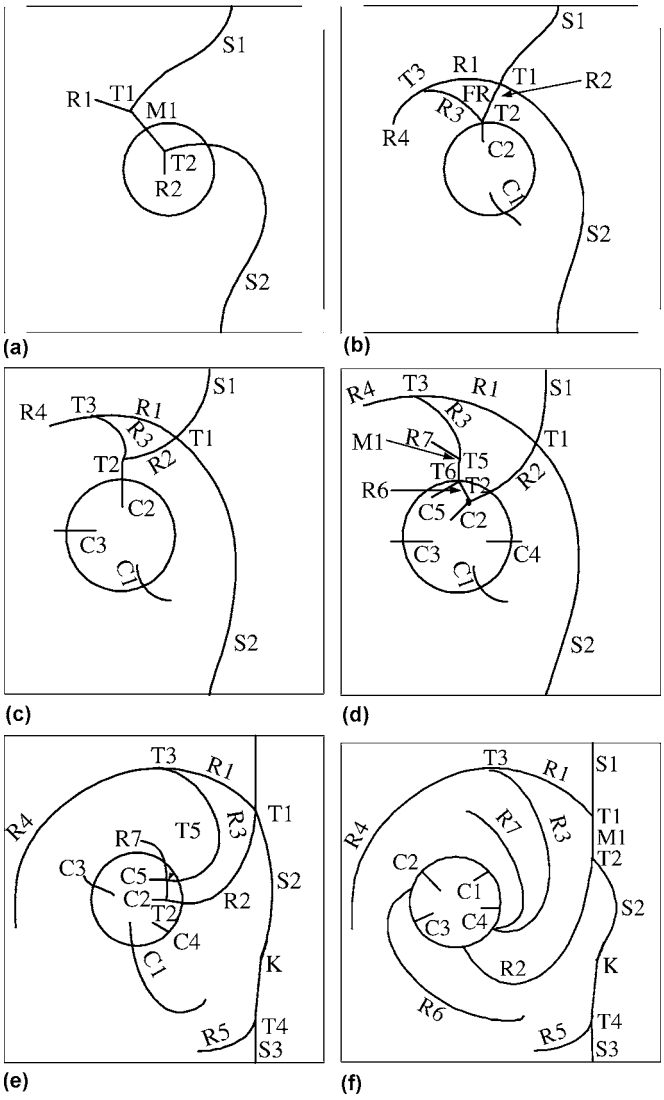

FIG. 4. Schematic pattern of the flow structure.

formed vortex. The secondary interaction between the reflected shock wave $R2$ and the deformed vortex takes place.

The secondary interaction is very similar to the first-stage interaction. It results in the deformation of the reflected shock wave and the vortex. The reflected shock wave $R2$ is distorted and separated by the vortex. It seems that there is another shock wave $C1$ at the opposite side of the vortex core [see Figs. 3(c) and 4(b)]. Because the reflected shock wave $R2$ moves clockwise and the vortex rotates counterclockwise, the tip part of $R2$ is decelerated. A secondary triple point $T2$ and a reflected shock wave $R3$ are formed. This pattern is presented in Figs. 3(d) and 4(b). The tip of $R3$ merges with the tip part of the reflected shock wave $R1$. Three reflected shock waves, $R1$, $R2$, and $R3$ form a triangle region that appears as a shock-focusing region, FR, which is similar to that observed by Pirozzoli *et al.*[23] and Inoue and Hattori[18] in the simulation of the interaction between a shock wave and two counter-rotating vortices and by Sturtevant and Kulkarny[35] in the experiment for the reflection of a weak shock wave. Similar to the first-stage interaction, the reflected shock wave $R2$ compresses the deformed vortex in the secondary interaction. The locally compressed region forms a shocklet $C3$ near the vortex center that is shown in Figs. 3(e) and 4(c). The development of the secondary interaction between the reflected shock wave and the deformed vortex results in the formation of new Mach stem, $M1$, two triple points, $T5$ and $T6$, and two more reflected shock waves near the root of the reflected shock wave $R3$; see Figs. 3(f) and 4(d). As time increases, the two triple points, $T5$ and $T6$, meet together. One of the reflected shock waves $R7$ moves toward $R3$. Another reflected shock wave forms a new shocklet in the vortex core. As can be seen in Figs. 3(g) and 4(e), five shocklets are formed in the near region of the vortex center. As the shocklets become stronger, they interact with the deformed vortex and the third stage of the interaction takes place; see Figs. 3(g), 3(h), 4(e), and 4(f).

The evolution of the shock structure reveals that the interaction of a shock wave and a strong vortex has a multistage feature including the interactions between the incident shock wave and the initial vortex, between the reflected shock wave and the deformed vortex, and between the shocklets and the deformed vortex. This multistage interaction will result in the multistage deformation of the vortex and a new mechanism of sound generation.

2. The shock structure of case F

The evolution of the shock structure in case F is shown in Fig. 5. Similar to the interaction in case A, the interaction of case F is also multistage. The secondary interaction of the reflected shock wave $R2$ and the deformed vortex takes place in Fig. 5(a) and generate shocklets. The shocklets interact with the deformed vortex and the third-stage interaction is formed. The difference between the interactions in case F and in case A is the type of the reflected shock wave, which is a regular reflection in case F but a Mach reflection in case A. The number of the shocklets in case F is smaller than that in case A, due to the weaker strength of the secondary interaction in case F.

3. Condition for the appearance of a multistage interaction

We have systematically studied the condition for the appearance of a multistage interaction between a shock wave and a strong vortex. To save space, we plot only the evolution of the vorticity of case A in Fig. 6, which is obtained by a third-order Runge–Kutta integration. Because interactions produce vorticity,[27,36,37] multiple peaks in the evolution of the vorticity can predict the appearance of a multistage interaction. As can be seen from Fig. 6, there are three peaks: $P1$, $P2$, and $P3$ corresponding to the time $t=3.43$, 4.62, and 8.15, respectively. A comparison with the evolution of the interaction in Fig. 3 reveals that these peaks result from the first, second, and third stages of the interaction, respectively. For the interaction of a shock wave with a weak vortex, no reflected shock wave can interact with the vortex. Only one stage interaction appears, resulting in only one peak in the evolution of the vorticity at the vortex center. Therefore, the variation of the vorticity at the vortex center could be a cri-

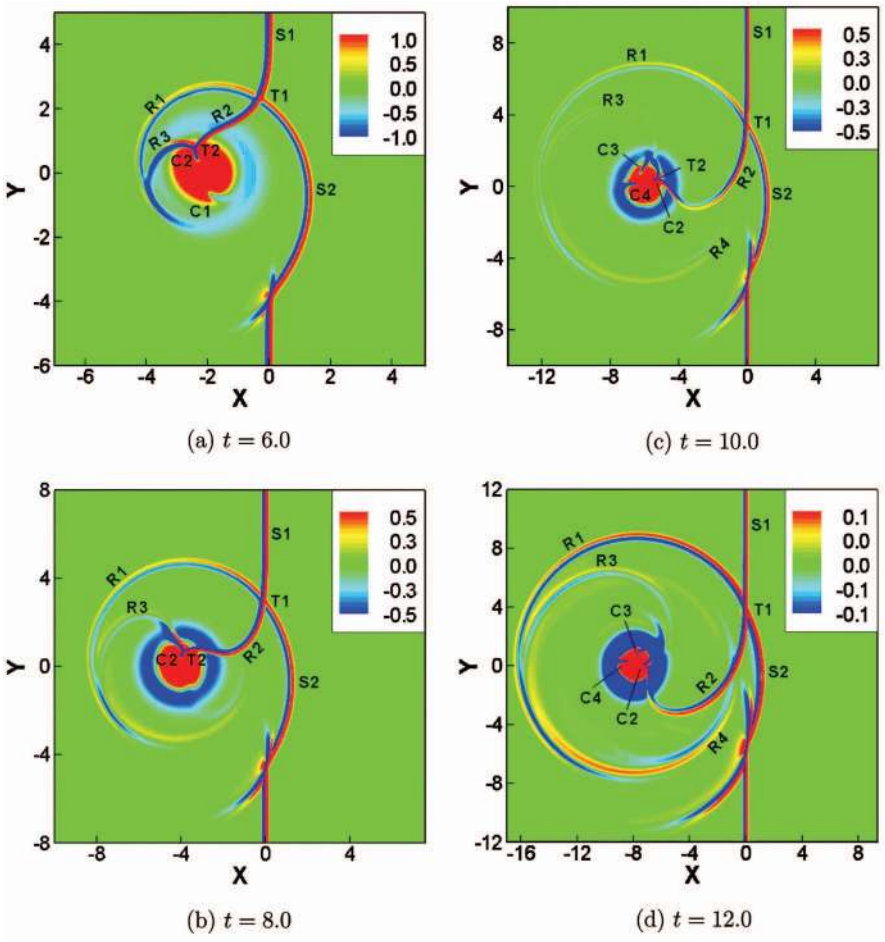

FIG. 5. (Color). The shock structure for case F: numerical shadowgraph obtained from $\nabla^2\rho$.

terion to judge the appearance of the secondary and third interactions of the reflected shock, shocklets, and the deformed vortex.

Figure 7 is the evolution of the vorticity at the vortex center for all simulation cases listed in Table I. Figure 7(a) contains the cases for $M_s=1.2$ and Fig. 7(b) contains the cases for $M_s=1.05$. In the case of $M_s=1.2$, there are three peaks in the evolution of the vorticity when $M_v \geqslant 0.7$. The multistage interaction will occur at $M_v \geqslant 0.7$. Figure 7(b) reveals that the multistage interaction occurs at $M_v \geqslant 0.8$ in the case of $M_s=1.05$. Stronger vortices are required for multistage interactions with a lower shock Mach number.

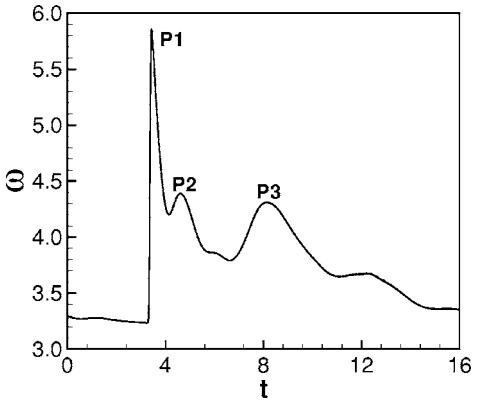

FIG. 6. Evolution of the vorticity at the vortex center for case A.

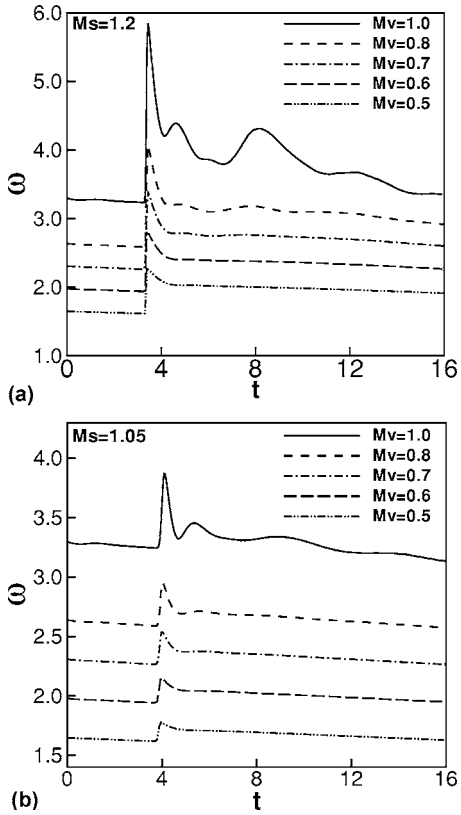

FIG. 7. The vorticity of the vortex center for different cases. (a) $M_s=1.2$; (b) $M_s=1.05$.

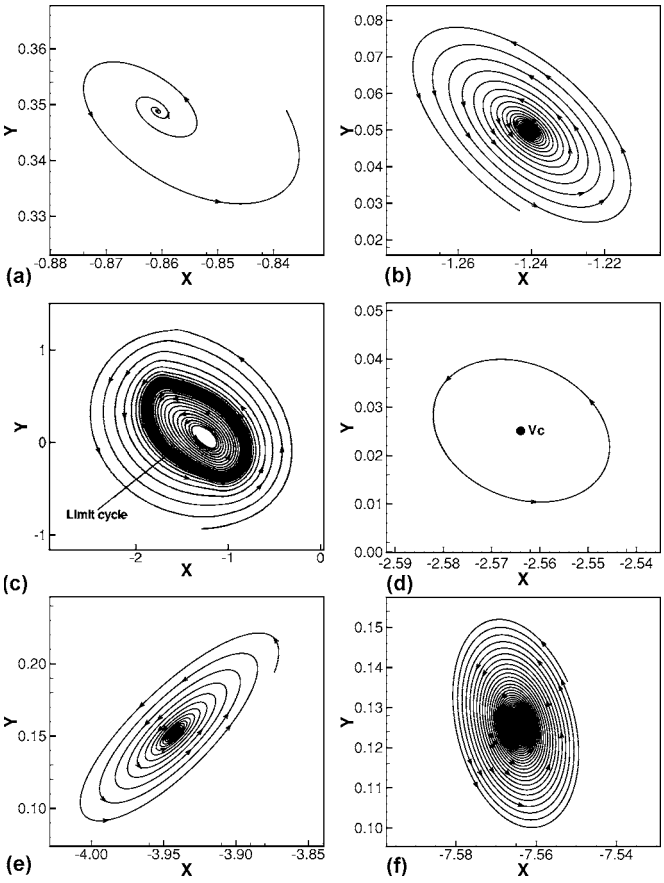

FIG. 8. Streamlines of the flow field near the vortex center defined as the critical point. (a) $t=4.0$; (b) $t=5.0$; (c) limit cycle at $t=5.0$; (d) $t=6.2$; (e) $t=8$; (f) $t=12$.

B. Vortex deformation and movement

1. Vortex deformation

Vortex deformation is an important feature of the shock–vortex interaction. The multistage interaction of a shock wave and a strong vortex results in the evolution of the vortex deformation having a multistage feature. Figure 8 shows the development of the streamlines for the perturbation velocity (u',v) of case A. Here, $u'=u-u_s$ and u_s is the velocity component in the x direction behind the incident shock wave. It reveals the following features different from those in an interaction between a shock and a weak vortex.

First, the initially circular vortex is compressed into a strong spiral shape and then to an elliptical shape. In the interaction of a shock wave and a weak vortex, the vortex is compressed into an elliptical shape just after it has passed the incident shock wave. In the interaction of a shock wave and a strong vortex, as can be seen from Fig. 8(a), the streamlines spiral outward quickly. At this early stage, it has a strong spiral shape rather than an elliptical shape. As time increases, the strong spiral vortex is gradually compressed into an elliptical shape as in Fig. 8(b).

Second, the evolution of the ratio of major to minor axes has a multistage feature. The ratio is computed by the following method: (1) We draw the major and minor axes in the picture of streamlines. (2) Choosing five points on the major and minor axes, respectively, we compute the lengths of both the major and the minor axes according to the equation of an ellipse. Five values are obtained for the ratio. (3) We average these five values to obtain the ratio of major to minor axes. The results are listed in Table II. There are three extrema. The first is a local maximum of 2.17 that occurs at $t=5.0$. A comparison with the evolution of the shock structure reveals that it results from the first-stage interaction between the incident shock wave and the initial vortex. The second is a local minimum of 1.08 at $t=6.6$. It is the effect of the second-stage interaction between the reflected shock wave and the deformed vortex. It is interesting to notice that the elliptical vortex is compressed back to an almost circular shape by the second-stage interaction. The third is a local maximum of 3.47 at $t=8$, which results from the third-stage interaction between the shocklets and the deformed vortex.

TABLE II. The ratio of major to minor axes at different time t.

Time	5.0	6.2	6.4	6.6	6.8
Ratio	2.17	1.35	1.20	1.08	1.14
Time	7.0	7.2	7.4	7.6	7.8
Ratio	1.46	1.79	1.91	2.39	2.74
Time	8.0	10.0	12.0	14.0	16.0
Ratio	3.47	1.83	1.72	1.54	1.63

The third different feature is that the deformed vortex does not rotate by a constant angular velocity. We measure the angle between the major axis and the y axis, with a positive angle for counterclockwise. This angle is approximately 135°, 155°, 45°, and 100° corresponding to the times $t=5$, 6.2, 8, and 12, respectively. It is obvious that the deformed vortex does not rotate at a constant angular velocity. This is different from the result in the interaction of a shock wave and a weak vortex in which the elliptical vortex rotates in a constant angular velocity (for $t\geqslant 4.0$ in Ref. 21).

2. Topological structure of the vortex

The topological structure of a vortex is characterized by the spiral direction and the existence of limit cycles in the near region of the vortex center.[38–40] It is an important part of the flow structure and could influence the secondary interaction appearing in the interaction of a shock and a strong vortex. However, it has not been discussed in previous studies on the problem of shock–vortex interaction.

The perturbation velocity near the vortex center can be written by a Taylor expansion as follows:

$$u' \approx \left(\frac{\partial u'}{\partial x}\right)_c x + \left(\frac{\partial u'}{\partial y}\right)_c y, \quad v \approx \left(\frac{\partial v}{\partial x}\right)_c x + \left(\frac{\partial v}{\partial y}\right)_c y, \quad (2)$$

where the subscript c represents the value at the vortex center. The streamlines can be described by the ordinary differential equation:

$$\frac{dy}{dx}=\frac{v}{u}=\frac{\left(\frac{\partial v}{\partial x}\right)_c x+\left(\frac{\partial v}{\partial y}\right)_c y}{\left(\frac{\partial u'}{\partial x}\right)_c x+\left(\frac{\partial u'}{\partial y}\right)_c y}. \tag{3}$$

For this ordinary differential equation, the condition for the critical point ($u'=0$, $v=0$) to be a vortex is $\Delta=4\bar{q}-\bar{p}^2>0$, where $\bar{q}=(\partial v/\partial x)_c(\partial u'/\partial y)_c-(\partial u'/\partial x)_c(\partial v/\partial y)_c$ and $\bar{p}=-[(\partial u'/\partial x)_c+(\partial v/\partial y)_c]$. $\bar{p}$ is an important parameter to determine the topological structure of a vortex. If $\bar{p}<0$, the streamlines spiral outward. If $\bar{p}=0$, the critical point is a center. If $\bar{p}>0$, the streamlines spiral inward.[41]

Based on the continuity equation, we obtain

$$\bar{p}=-\left[\left(\frac{\partial u'}{\partial x}\right)_c+\left(\frac{\partial v}{\partial y}\right)_c\right]=\frac{1}{\rho}\left(\frac{\partial \rho}{\partial t}+u_s\frac{\partial \rho}{\partial x}\right)_c$$
$$=\frac{1}{\rho}\left(\frac{\partial \rho}{\partial t}+\frac{u_s}{RT}\frac{\partial p}{\partial x}-\frac{\rho u_s}{T}\frac{\partial T}{\partial x}\right)_c, \tag{4}$$

where T is the temperature and R is a gas constant. The first term on the right-hand side of (4) represents the unsteady effect, and the last two terms represent the baroclinic effect. In our case, the interaction of a shock wave with a strong vortex results in an unsteady movement of the vortex (we will discuss this later). As a result, $\bar{p}$ is a function of time and the vortex takes a spiral shape. For vortical flow, the streamlines in the outer region of the vortex core spiral inward. If the streamlines in the inner region spiral outward, there exists a stable limit cycle near the vortex center. In the evolution of the vortex in case A, $\bar{p}$ equals −0.826, −0.088, 0.000, 0.093, and 0.040 corresponding to the time $t=4.0$, 5.0, 6.2, 8.0, and 12.0, respectively. Figures 8(a) and 8(b) are outward spiraling streamlines at $t=4.0$ and 5.0, respectively, while $\bar{p}$ is negative. At these instants, there exists a stable limit cycle. Figure 8(c) is an example for $t=5.0$. Figure 8(d) contains closed streamlines at $t=6.2$ with $\bar{p}=0.000$. The outward spiral types are shown in Figs. 8(e) and 8(f) for $t=8$ and $t=12$.

3. Vortex center

All the features discussed above about the vortex deformation, especially the topological structure, are strongly related to the definition of the vortex center. There are three methods used in the literature to define the vortex center. The first is the point of local minimum density where both the spatial derivatives of the density vanish ($\partial\rho/\partial x=0$, $\partial\rho/\partial y=0$). The vortex center determined from the density contour, the shadowgraph, or the schlieren and interferogram[2] are related to this method. The second is the point of local minimum pressure.[42] The last is the critical point in the streamlines where the two components of the perturbation velocity vanish.[42] For a steady polytropic flow, the three definitions will give the same vortex center. But after the vortex interacts with the incident shock wave, the expansion and baroclinic effects will influence the flow significantly. The gradients of density and pressure are not aligned. The vortex is not steady anymore. Hence, the three methods will give different results for the vortex center. We compute the vortex center based on these three methods. In addition, we integrate the trajectory of the vortex center by a third-order Runge–Kutta method. The results plotted in Fig. 9 show a significant difference among the three methods during the interaction of the shock wave and the vortex. In addition, it is interesting to note that there is an oscillatory movement around the horizontal line, $y\approx 0.15$. This is the result of a nonlinear effect of the shock vortex interaction.[22] Figure 10 is vorticity contours in which we pinpoint the vortex center. Much difference is observed at $t=5$ and 8 when the second- or third-stage interaction is in its strongest time.

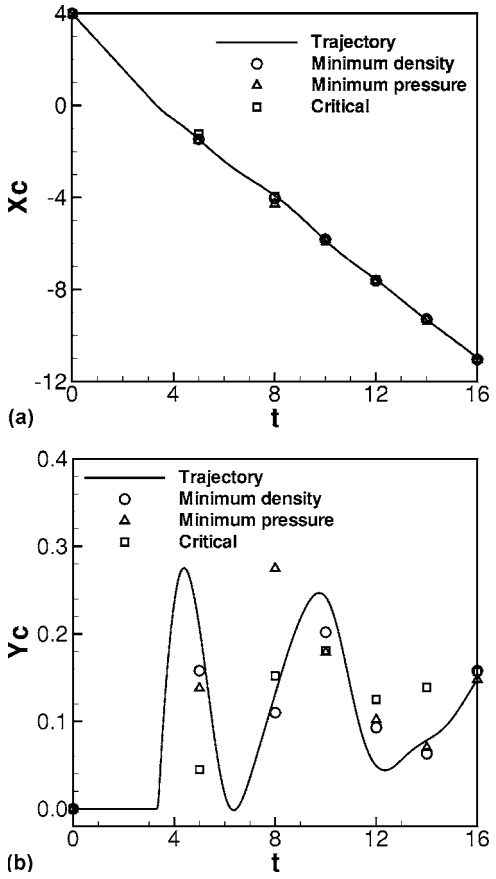

FIG. 9. The trajectory of the vortex center (solid line) and the comparison among different definitions based on the points of local minimum density ○, local minimum pressure △, and critical point □. (a) x_c; (b) y_c.

The topological structure of the vortex using different definitions for the vortex center may be different. Figure 11 is the (perturbation) streamlines near the vortex center defined as the point of the local minimum pressure for case A at $t=5.0$. It is totally different from that in Fig. 8(b). The reason is that the point of the local minimum pressure is far from the critical velocity point [see Fig. 9(b) and Fig. 10(a)]. The gradient of the divergence is high near the vortex center. For instance, $\bar{p}=-0.088$ at the critical point (−1.241, 0.045). It is −0.004 at the point (−1.517, 0.138) of the local minimum pressure. The effect of the definition of the vortex center on the other two features of the vortex deformation is not so significant.

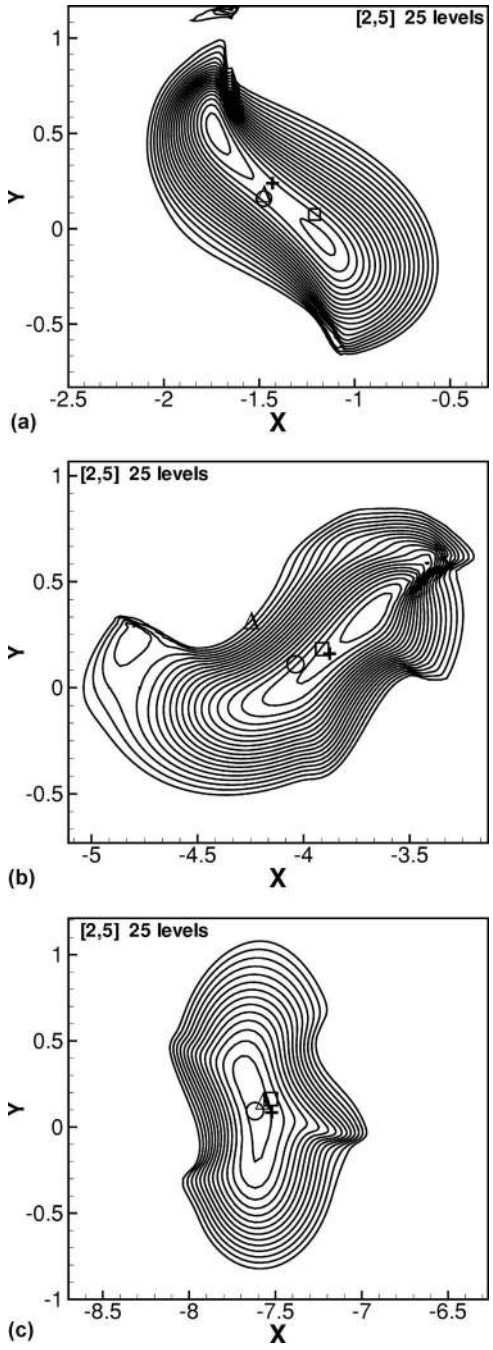

FIG. 10. Contours of vorticity and the vortex center obtained from the different definition based on the points of local minimum density ○, local minimum pressure △, critical point □, and trajectory +. (a) $t=5$; (b) $t=8$; (c) $t=12$.

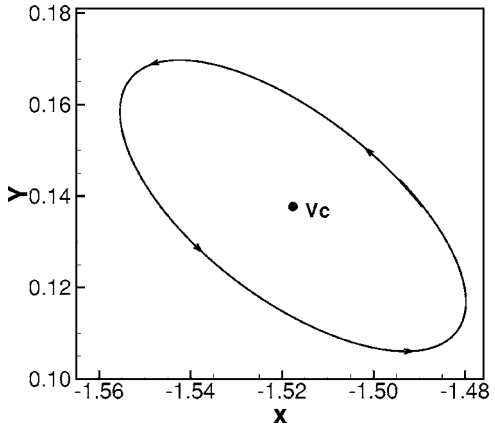

FIG. 11. Streamlines near the vortex center defined as the local pressure minimum at $t=5.0$.

C. Sound generation and propagation

The generation and propagation of sound waves are the most interesting phenomena in the shock vortex interaction problem. It has been studied extensively.[2,4–6,12–14,18,19,21–23,25,27] However, for the problem of shock interacting with a strong vortex, the multistage interactions result in a different mechanism of the generation of sound waves.

Following the previous study,[18] we define the sound pressure as $\Delta p=(p-p_s)/p_s$, where p_s is the mean pressure behind the incident shock wave. Figure 12 shows the evolution of the sound pressure for case A (left) and case F (right) at typical times. It indicates that the development of sound waves of these two cases are similar. In this figure, the symbol $\oplus$ denotes the compression region ($\Delta p>0$), while $\ominus$ denotes the rarefaction region ($\Delta p<0$). The early stage for the generation of sound waves is not plotted because it was discussed in great detail in the previous studies[18,21] for weak vortices and there is no qualitative difference between the cases of strong and weak vortices. We draw the pictures for the later stage to focus our study on the sound generation of the multistage interaction unique to the interaction between shocks and strong vortices.

Similar to the shock weak vortex interaction,[19] three sound waves are observed that are generated by the first-stage interaction between the incident shock wave and the initial vortex. A different feature is that the reflected shock waves that are generated by the secondary interaction are embedded in the sound waves. It results in the interaction of sound waves with the reflected shock waves. As can be seen from the left pictures of Fig. 12, the reflected shock wave $R1$ elongates circumferentially and swirls around the vortex. The precursor is located ahead of $R1$. The second sound wave is located behind $R1$. The shock-focusing region becomes part of the second sound wave. As time increases, the sound waves radiate from the vortex center. At $t=12$, both reflected shock waves $R2$ and $R3$ are embedded in the second sound wave. The third sound wave is generated. The reflected shock wave $R7$ is located between the second sound wave and the third sound wave. The second sound wave is located ahead of $R7$ and the third sound wave is located behind $R7$. This configuration is similar to the configuration of the precursor, $R1$ and the second sound wave. Since the secondary reflected shock waves $R3$ and $R7$ are formed in the secondary interaction; this structure cannot be observed in the interaction of the shock wave with weak vortices.

The multistage interaction strongly suggests that the interaction of a shock wave and a strong vortex should produce more sound waves due to the secondary interaction. Unfortunately, we have not observed new sound waves. We suspect that this is due to the limited size of the simulation

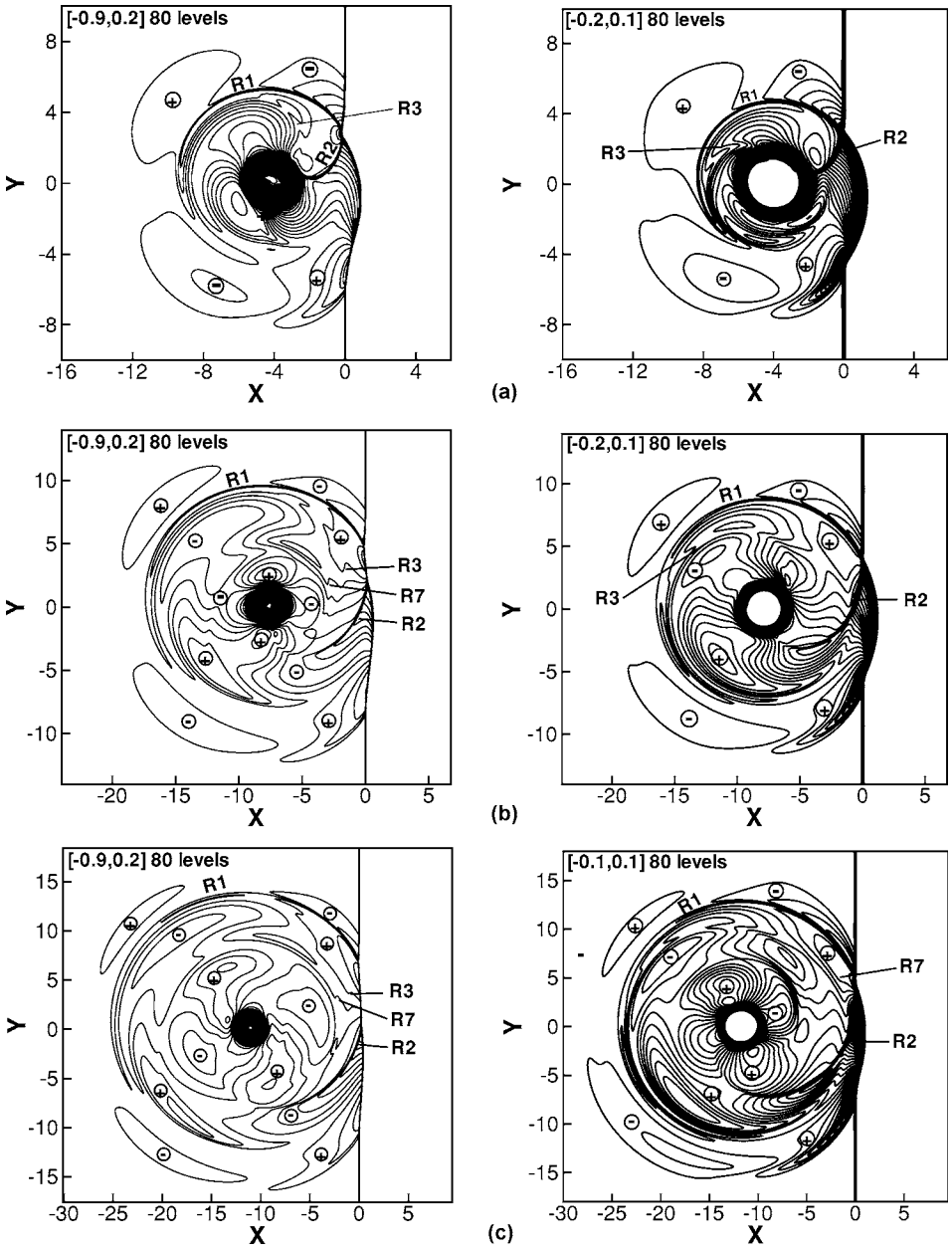

FIG. 12. Sound pressure field. Left: $M_s=1.2$; right: $M_s=1.05$. (a) $t=8.0$; (b) $t=12$; (c) $t=16$.

domain and limited simulation time. The confirmation of more sound waves from the secondary interaction is left for future work.

Figure 13(a) shows the distribution of the sound pressure jump Δp against the distance from the vortex center for a fixed angle $\theta^*=-45°$ at $t=12$ and 16 of case A. It is interesting to see that the reflected shock wave $R1$ produces a pressure jump between the precursor and the second sound wave. It is much higher than the peak of the precursor. The reflected shock wave $R7$ produces a pressure peak at $r\approx 10$ between the second and third sound waves. Figure 13(b) is the circumferential distribution of the sound pressure Δp for the precursor ($r=16.0$), second sound wave ($r=12.0$), and third sound wave ($r=6.7$) at $t=16$. Comparing with the case of a weak vortex [see Fig. 2(b)], a significant difference can be observed. There are three more turning points at $\theta^*=-130°$, 70°, and 80° in the second sound wave that are the effects of shock waves $R3$, $R7$, and $R2$, respectively. The third sound wave is also influenced by the shock wave $R2$, which is represented as a weak turning point at $\theta^*=70°$.

V. CONCLUDING REMARKS

The interaction of a shock wave with a strong vortex is systematically simulated through solving the two-dimensional, unsteady compressible Navier–Stokes equations. The effect of the strengths of shock waves and vortices on the flow field is examined. The results show that the strong reflected shock wave generated by the interaction of the incident shock wave and the initial vortex can interact with the deformed vortex and form a secondary interaction. The secondary interaction generates shocklets in the near region of the vortex center that interact with the deformed vortex and form a third-stage interaction. The interaction of a shock wave and a strong vortex has a multistage feature. The condition for the appearance of the multistage interaction is

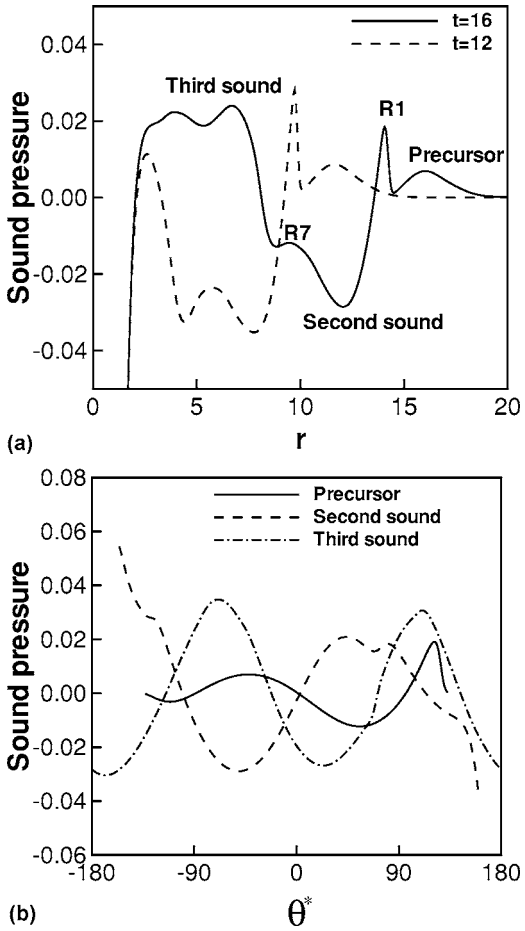

FIG. 13. Radial and circumferential distribution of the sound pressure ∇p. (a) Radial distribution at $\theta^*=-45°$; (b) circumferential distribution at $t=16$.

obtained by a parameter study. A stronger vortex is required for a multistage interaction to appear for a lower shock Mach number.

Deformation of the vortex also has a multistage feature. The initial circular vortex is first compressed to a strong spiral shape and then gradually compressed to an elliptical shape in the first stage of interaction. The deformed vortex is compressed back to a nearly circular shape in the second stage of interaction. It is compressed to an elliptical shape again in the third stage of interaction.

Interactions seem to appear between reflected shock waves and sound waves. Several reflected shock waves that are generated in the second stage of interaction are embedded in the second and third sound waves. The multistage interaction suggests that there should exist more sound waves generated by the second and third stages of interaction. Unfortunately, we have not observed such new sound waves. We suspect that this is due to the limited size of the simulation domain and limited simulation time. The confirmation of more sound waves from the secondary interaction is left for future work.

ACKNOWLEDGMENTS

The computation was supported by the Boston University Scientific Computing Facilities (SCF) and by the Brown University Technology Center for Advanced Scientific Computing and Visualization (TCASCV). This research was partially supported by the Chinese Academy of Sciences while C.-W.S. was in residence at the University of Science and Technology of China (Grant No. 2004-1-8) and at the Institute of Computational Mathematics and Scientific/Engineering Computing. Additional support was provided by ARO Grant No. W911NF-04-1-0291, NSF Grants No. DMS-0207451 and No. DMS-0510345, and AFOSR Grant No. FA9550-05-1-0123.

[1] M. A. Hollingsworth and E. J. Richards, "A schlieren study of the interaction between a vortex and a shock wave in a shock tube," Aeronautical Research Council Rept. 17985, Fluid Motion Subcommittee, 2323, 1955.
[2] D. S. Dosanjh and T. M. Weeks, "Interaction of a starting vortex as well as a vortex street with a traveling shock wave," AIAA J. **3**, 216 (1965).
[3] A. Naumann and E. Hermanns, "On the interaction between a shock wave and a vortex field," AGARD Conf. Proc. **131**, 23.1 (1973).
[4] H. S. Ribner, "The sound generated by interaction of a single vortex with a shock wave," University of Toronto, Institute of Aerospace Studies, UTIA Report No. 61, 1959.
[5] H. S. Ribner, "Cylindrical sound wave generated by shock-vortex interaction," AIAA J. **23**, 1708 (1985).
[6] T. M. Weeks and D. S. Dosanjh, "Sound generation by shock-vortex interaction," AIAA J. **5**, 660 (1967).
[7] M. J. Lighthill, "On sound generated aerodynamically I: General theory," Proc. R. Soc. London, Ser. A **211**, 564 (1952).
[8] N. Curle, "The influence of solid boundaries upon aerodynamic sound," Proc. R. Soc. London, Ser. A **231**, 505 (1955).
[9] L. Ting, "Transmission of singularities through a shock wave and the sound generation," Phys. Fluids **17**, 1518 (1974).
[10] L. Guichard, L. Vervisch, and P. Domingo, "Two-dimensional weak shock-vortex interaction in a mixing zone," AIAA J. **33**, 1797 (1995).
[11] S. K. Lele, "Compact finite difference schemes with spectral-like resolution," J. Comput. Phys. **103**, 16 (1992).
[12] J. L. Ellzey, M. R. Henneke, J. M. Picone, and E. S. Oran, "The interaction of a shock with a vortex: Shock distortion and the production of acoustic waves," Phys. Fluids **7**, 172 (1995).
[13] J. L. Ellzey and M. R. Henneke, "The shock-vortex interaction: the origins of the acoustic wave," Fluid Dyn. Res. **21**, 171 (1997).
[14] J. L. Ellzey and M. R. Henneke, "The acoustic wave from a shock-vortex interaction: Comparison between theory and computation," Fluid Dyn. Res. **27**, 53 (2000).
[15] J. P. Boris and D. L. Book, "Solution of the continuity equation by the method of flux-corrected transport," Methods Comput. Phys. **16**, 85 (1967).
[16] J. P. Boris, A. M. Landsberg, E. S. Oran, and J. H. Gardner, "LCPFCT—a flux-corrected transport algorithm for solving generalized continuity equations," NRL Memorandum Report No. 6410-93-7192, 1993.
[17] M. R. Henneke and J. L. Ellzey, "The effect of a shock on vortex interactions," Proceedings of the 19th International Symposium on Shock Waves, 26–30 July 1993, Marseilles, France.
[18] O. Inoue and Y. Hattori, "Sound generation by shock-vortex interactions," J. Fluid Mech. **380**, 81 (1999).
[19] O. Inoue, "Propagation of sound generated by weak shock-vortex interaction," Phys. Fluids **12**, 1258 (2000).
[20] F. Grasso and S. Pirozzoli, "Shock wave–thermal inhomogeneity interactions: Analysis and numerical simulations of sound generation," Phys. Fluids **12**, 205 (2000).
[21] F. Grasso and S. Pirozzoli, "Shock-wave-vortex interactions: Shock and vortex deformations, and sound production," Theor. Comput. Fluid Dyn. **13**, 421 (2000).
[22] G. Erlebacher, M. Y. Hussaini, and T. L. Jackson, "Nonlinear strong shock interactions: A shock-fitted approach," Theor. Comput. Fluid Dyn. **11**, 1 (1998).
[23] S. Pirozzoli, F. Grasso, and A. D'Andrea, "Interaction of a shock wave with two counter-rotating vortices: Shock dynamics and sound production," Phys. Fluids **13**, 3460 (2001).
[24] O. Inoue and Y. Takahashi, "Successive generation of sounds by shock-strong vortex interaction," Phys. Fluids **12**, 3229 (2000).
[25] O. Inoue, T. Takahashi, and N. Hatakeyama, "Separation of reflected

shock waves due to secondary interaction with vortices: Another mechanism of sound generation," Phys. Fluids **14**, 3733 (2002).
[26]F. J. Barbosa and B. W. Skews, "Shock wave interaction with a spiral vortex," Phys. Fluids **13**, 3049 (2001).
[27]A. Rault, G. Chiavassa, and R. Donat, "Shock-vortex interactions at high Mach numbers," J. Sci. Comput. **19**, 347 (2003).
[28]R. Donat and A. Marquina, "Capturing shock reflections: An improved flux formula," J. Comput. Phys. **125**, 42 (1996).
[29]G.-S. Jiang and C.-W. Shu, "Efficient implementation of weighted ENO schemes," J. Comput. Phys. **126**, 202 (1996).
[30]C.-W. Shu, "Essentially non-oscillatory and weighted essentially non-oscillatory schemes for hyperbolic conservation laws," in *Advanced Numerical Approximation of Nonlinear Hyperbolic Equations*, Lecture Notes in Mathematics, edited by B. Cockburn, C. Johnson, C.-W. Shu, E. Tadmor, and A. Quarteroni (Springer, New York, 1998), Vol. 1697, pp. 325–432.
[31]C.-W. Shu and S. Osher, "Efficient implementation of essentially non-oscillatory shock capturing schemes," J. Comput. Phys. **77**, 439 (1988).
[32]J. Shi, Y.-T. Zhang, and C.-W. Shu, "Resolution of high order WENO schemes for complicated flow structures," J. Comput. Phys. **186**, 690 (2003).
[33]Y.-T. Zhang, J. Shi, C.-W. Shu, and Y. Zhou, "Numerical viscosity and resolution of high-order weighted essentially nonoscillatory schemes for compressible flows with high Reynolds numbers," Phys. Rev. E **68**, 046709 (2003).
[34]G. Erlebacher, M. Y. Hussaini, and C.-W. Shu, "Interaction of a shock with a longitudinal vortex," J. Fluid Mech. **337**, 129 (1997).
[35]B. Sturtevant and V. A. Kulkarny, "The focusing of weak shock waves," J. Fluid Mech. **73**, 651 (1976).
[36]N. K.-R. Kevlahan, "The vorticity jump across a shock in a non-uniform flow," J. Fluid Mech. **341**, 371 (1997).
[37]J. M. Picone and J. P. Boris, "Vorticity generation by shock propagation through bubbles in a gas," J. Fluid Mech. **189**, 23 (1988).
[38]A. E. Perry and M. S. Chong, "A series-expansion study of the Navier–Stokes equations with applications to three-dimensional separation patterns." J. Fluid Mech. **173**, 207 (1986).
[39]A. E. Perry and T. R. Steiner, "Large-scale vortex structures in turbulent wakes behind bluff bodies. Part 1. Vortex formation process," J. Fluid Mech. **174**, 233 (1987).
[40]M. Tobak and D. J. Peake, "Topology of three-dimensional separated flows," Annu. Rev. Fluid Mech. **14**, 61 (1982).
[41]J. Crank, H. G. Martin, and D. M. Melluish, *Nonlinear Ordinary Differential Equations* (Oxford University Press, Oxford, 1977).
[42]J. Jeong and F. Hussain, "On the identification of a vortex," J. Fluid Mech. **285**, 69 (1995).